Applied Catalysis B: Environmental 130–131 (2013) 285–292

Contents lists available at SciVerse ScienceDirect

Applied Catalysis B: Environmental

journal homepage: www.elsevier.com/locate/apcatb

Photocatalytic degradation of carbamazepine by tailored $BiPO_4$: efficiency, intermediates and pathway

Jian Xu[a,b], Lei Li[a,b], Changsheng Guo[a,b], Yuan Zhang[a,b,*], Wei Meng[a,b]

[a] State Key Laboratory of Environmental Criteria and Risk Assessment, Chinese Research Academy of Environmental Sciences, Beijing 100012, China
[b] Laboratory of Riverine Ecological Conservation & Technology, Chinese Research Academy of Environmental Sciences, Beijing 100012, China

ARTICLE INFO

Article history:
Received 8 August 2012
Received in revised form 8 November 2012
Accepted 11 November 2012
Available online 23 November 2012

Keywords:
Photocatalysis
$BiPO_4$
Carbamazepine
Intermediates
Pathway

ABSTRACT

This study firstly explored the photodegradation of carbamazepine, one of the most frequently detected pharmaceuticals, with tailored $BiPO_4$ nanomaterials. $BiPO_4$ was synthesized with a hydrothermal method. The physicochemical properties of the obtained samples were characterized and the results indicated that both the hydrothermal temperature and reaction time influenced the phase, morphology and optical properties of the $BiPO_4$ catalysts, which may further determine their specific photocatalytic performances. The intrinsic microstructure and optical properties reflected the crystal properties of the catalysts to some extent. The $BiPO_4$ prepared at 180 °C for 72 h (BPO-180-72) displayed the best photocatalytic activity under UV irradiation, during which carbamazepine was nearly completely eliminated from ultrapure water after 60 min irradiation. The good photocatalytic activity was ascribed to the synergistic effect of monoclinic phase and relatively ordered morphology of the resulting $BiPO_4$. Particularly, the monoclinic phase was firstly proved to be more active than the hexagonal phase for $BiPO_4$ samples. BPO-180-72 removed approximately 72.4% of carbamazepine from lab-prepared simulated wastewater after 60 min irradiation, suggesting the potential application of this material in wastewater treatment. Ten reaction intermediate products were observed and identified by HPLC–MS/MS, and a tentative reaction pathway was proposed. Results indicated that photogenerated holes and hydroxyl radicals were the main reactive species for the photodegradation of carbamazepine in the system.

1. Introduction

The occurrence of pharmaceuticals and personal care products (PPCPs) in the environment is of increasing concern due to their high persistence during wastewater treatment processes [1–3]. Among various PPCPs, carbamazepine (5H-dibenzo[b,f]azepine-5-carboxamide) is one of the most frequently detected pharmaceuticals, which is prescribed for human medicine to control seizures. Carbamazepine is administered chronically to patients with a daily dosage of 100–2000 mg, resulting in high production around the world [4]. Approximately 50% of administrated carbamazepine and its metabolites excreted in urine and feces are directly released to the municipal wastewater treatment plants (WWTPs) [5], however, the removal efficiencies of carbamazepine in conventional WWTPs are very low due to its biorefractory nature.

Numerous studies have reported the presence of carbamazepine in environmental samples at relatively high concentrations [1,6]. To transform these compounds in to non-toxic and pharmaceutically inactive products, methods such as Fenton oxidation, ozonation, TiO_2 photocatalysis and other chemical oxidation processes are generally employed [2,3,7,8], of which photocatalytic oxidation by TiO_2 has become the most attractive clean alternative because of its economic and ecologically safe option for solving energy and pollution problems, and high degradation and mineralization efficiency [9–11]. However, there are some inherent drawbacks with traditional TiO_2 oxidation, such as the rapid recombination of charge carriers and the recovery of the reacted TiO_2 particles [11–13]. It was also reported that the relatively inefficient quantum yield and wide band gap of TiO_2 made it difficult for application at an industrial scale [13]. Bismuth-based nanostructured photocatalysts have been documented to show superior photocatalytic performances than traditional TiO_2 in both UV and visible light regions [14–16]. Bismuth phosphate ($BiPO_4$) as one of the Bi salts has potential applications in ion sensing, separating radioactive elements as well as catalysis [17]. The photocatalytic efficiency of $BiPO_4$ was well verified by the degradation of dyes, such as methyl orange (MO), methyl blue (MB) and rhodamine B (RhB) [14,17,18]. Pan et al. reported the photocatalytic performance of synthesized $BiPO_4$ oxy-acid salt on dyes degradation, and found the inductive role of PO_4^{3-} helped the e^-/h^+ separation and enhanced its photocatalytic activity [14]. The

* Corresponding author at: State Key Laboratory of Environmental Criteria and Risk Assessment, Chinese Research Academy of Environmental Sciences, Beijing 100012, China. Tel.: +86 10 84915237; fax: +86 10 84926073.
E-mail address: zhangyuan@craes.org.cn (Y. Zhang).

0926-3373/$ – see front matter © 2012 Elsevier B.V. All rights reserved.
http://dx.doi.org/10.1016/j.apcatb.2012.11.013

photocatalytic performance of $BiPO_4$ has been proven to be closely related to its crystalline phase, band gap, surface area and morphologies [17,18]. However, controllably synthesizing the desired catalysts with best activity under different experimental conditions was not systemically studied. Besides, the main targets of photocatalysis by $BiPO_4$ were dyes, and its ability to degrade PPCPs is not well understood.

The purpose of this study was to investigate the photocatalytic degradation of carbamazepine by fabricated $BiPO_4$ as a catalyst under UV irradiation. $BiPO_4$ was synthesized by hydrothermal method, taking into account variables such as hydrothermal temperature and reaction time, since both factors play important roles in simultaneously controlling the size, morphology, and dispersivity of the nanocrystals [15]. The synthesized materials were comprehensively characterized by field emission scanning electron microscope (FESEM), transmission electron microscopy (TEM), X-ray diffraction (XRD), ultraviolet–visible spectroscopy (UV–vis) and X-ray photoemission spectroscopy (XPS) techniques. Liquid chromatography–tandem mass spectrometry (LC–MS/MS) was used to identify the reaction intermediates of carbamazepine, and a tentative reaction pathway was proposed. Additionally, the removal efficiency of carbamazepine in simulated wastewater was also studied by $BiPO_4$ catalyst with the best catalytic performance, in the view of practical applications.

2. Experimental design

2.1. Materials

Carbamazepine standard (purity > 99%) was purchased from Sigma–Aldrich (St. Louis, MO, USA). The chemicals used for the mobile phase for HPLC–MS analysis included Milli-Q ultrapure water and HPLC grade methanol (Dikma Chemical, China). Other chemicals and reagents, such as $Bi(NO_3)_3{\bullet}5H_2O$, $Na_3PO_4{\bullet}12H_2O$, NaOH, and HNO_3, were in analytical grade and used as received.

2.2. Synthesis and characterization of $BiPO_4$

$BiPO_4$ was synthesized via a simple hydrothermal method. Briefly, 1.14 g of $Na_3PO_4{\bullet}12H_2O$ was dissolved in 20 mL of ultrapure water, and 20 mL of 0.15 mol/L $Bi(NO_3)_3{\bullet}5H_2O$ stock solution was added drop-wise. The mixture (pH = 0.5) was magnetically stirred for 30 min at room temperature, and the obtained suspension was transferred to a 50 mL Teflon-lined autoclave. The influence of hydrothermal temperature and reaction time was investigated by putting the autoclave in the oven at different temperatures (140, 160, 180 and 200 °C) for different time courses (1, 4, 12, 24, 48, 72 and 96 h). After the autoclave naturally cooled down to room temperature, the products were collected and washed with distilled water and absolute ethanol several times, then air-dried at 60 °C for 12 h.

The phase composition of the obtained $BiPO_4$ catalysts was determined by a Rigaku D/Max-2500 diffractometer using Cu Kα radiation (λ = 1.54178 Å). The morphology and size of the catalysts were obtained by FESEM (FEI nanosem 430) and TEM (JEM-100CX II). The specific surface area, total pore volume, and average pore diameter were determined using the surface area and pore-size analyzer (Quantachrome NOVA 2000e). The optical properties of the products were recorded by a diffuse-reflectance UV–vis spectrometer (Shimadzu UV-3600), which was equipped with integrating spheres using $BaSO_4$ as a reference. XPS analysis was performed by a Kratos Axia Ultra DLD spectrometer with a monochromated Al Kα X-ray source ($h\nu$ = 1489.6 eV).

2.3. Photocatalytic reaction

The photocatalytic degradation experiments were performed in a photochemical reactor (XPA-2, Nanjing Xujiang Machinery Factory, Nanjing, China). The UV irradiation was supplied by a 100 W mercury lamp (Institute of Electric Light Source, Beijing, China), which was positioned in the middle of a cylindrical quartz trap. A quantity of 0.2 g of $BiPO_4$ catalyst was added into 200 mL carbamazepine solution (5 mg/L). Prior to irradiation, the suspension was magnetically stirred in darkness for 30 min to achieve adsorption–desorption equilibrium of carbamazepine on $BiPO_4$ (a preliminary study indicated that 30 min was sufficient time to achieve adsorption equilibrium). With the light on, an aliquot of 4 mL reaction solution was sampled at given time intervals. The solution was centrifuged at 3000 rpm for 5 min, and filtered through 0.45 μm nylon membrane prior to carbamazepine analysis. The removal efficiencies of carbamazepine were calculated by the following equation:

$$\text{Removal} = \frac{C_t}{C_0} \times 100\%$$

where C_0 and C_t represent the initial equilibrium concentration of carbamazepine and the reaction concentration at time t, respectively.

For comparison, simulated wastewater spiked with certain amounts of carbamazepine was conducted under the identical experimental conditions. The chemical composition of the simulated wastewater was referenced to the work of Postigo and co-authors, which met the guidelines established by both the United States Environmental Protection Agency (USEPA) and the Organization for Economic Co-operation and Development (OECD) for moderately hard synthetic freshwater and synthetic sewage, respectively [19]. Solid-phase extraction (SPE) was applied to extract carbamazepine from the simulated wastewater, during which the reaction solution passed through Oasis HLB cartridges (200 mg, 6 mL, Waters Corp., Milford, MA, USA), and the final residues were eluted with methanol.

2.4. Analysis of carbamazepine and its intermediates

The HPLC separation was performed using an Agilent 1200 series (Palo Alto, CA, USA) equipped with an Agilent Zorbax Eclipse XDB-C18 column (2.1 mm × 100 mm, 3.5 μm). The column was maintained at 30 °C during the sample analysis. The mobile phase consisted of eluent A (methanol) and eluent B (0.1% formic acid in ultrapure water). The flow rate was kept at 0.2 mL/min, and the injection volume was 10 μL. The separation of carbamazepine and its degradation intermediates were achieved with the following gradient program: 0–2 min: 30% A; 2–8 min: 30–70% A; 8–14 min: 70% A; 14–16 min: 70–30% A; 16–18 min: 30% A. The system was re-equilibrated for 10 min between runs. The concentration of carbamazepine was determined by HPLC-SIR-MS (Agilent 6410 triple quadrupole) equipped with an electrospray ionization source (ESI) in negative ionization mode for isolation of m/z at 237.1 ([M−H]- ion).

The identification of oxidative degradation intermediates in the solution was conducted by LC–MS and LC-SIR-MS equipped with electrospray ionization source, which was operated in the negative ionization mode. Selected ion recording (SIR) mode with a dwell time of 200 ms was used to acquire MS spectra of carbamazepine and its intermediates with a scan in the range of m/z 100–500. The nebulizer pressure was set to 35 psi and the flow rate of drying gas was 7 L/min. The capillary and nozzle voltages were 4000 and 0 V, respectively. The flow rate and temperature of the sheath gas were 8 L/min and 350 °C, respectively.

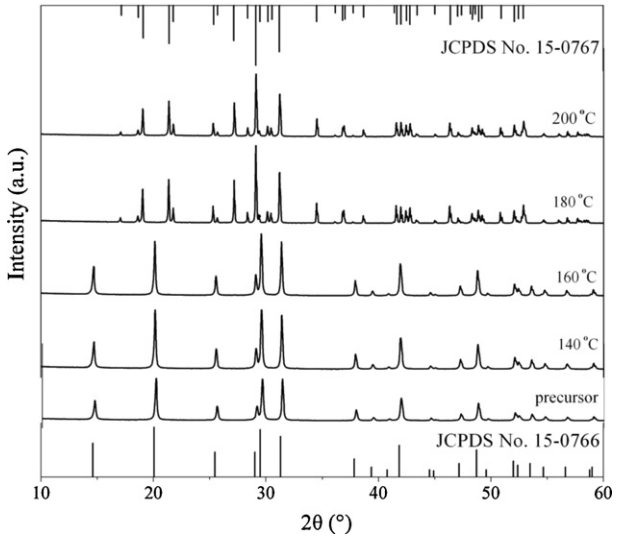

Fig. 1. XRD patterns of $BiPO_4$ samples prepared for 72 h at different temperatures.

The formation of the hydroxyl radical on the surface of the BPO-180-72 under UV light irradiation was recorded by the photoluminescence (PL) technique with terephthalic acid as a probe molecule, which can readily react with •OH to produce the highly fluorescent product, 2-hydroxyterephthalic acid [16]. The experimental procedure was similar to our previous work, and the fluorescence spectra of the formed 2-hydroxyterephthalic acid were measured by a Hitachi F-4500 spectrophotometer excited at 315 nm.

3. Results and discussion

3.1. Catalyst characterization

Figs. 1 and S1 show the XRD patterns of $BiPO_4$ samples prepared via hydrothermal procedure under different conditions. The diffraction peaks of the direct precipitate precursors before hydrothermal reaction matched well with the hexagonal phase $BiPO_4$ with lattice parameters of $a = b = 6.982$ and $c = 6.476$ Å (JCPDS No. 15-0766) (its standard image is shown at the bottom of Fig. 1). After hydrothermal treatment, the crystal phases of $BiPO_4$ prepared at 140 and 160 °C were indexed to pure hexagonal phase, while the $BiPO_4$ synthesized at 180 and 200 °C were pure monoclinic phase with $a = 6.752$, $b = 6.993$ and $c = 6.468$ Å (JCPDS 15-0767) (standard XRD pattern shown on the top of Fig. 1), due to the fact that the phase transformation occurred at 180 °C. The sharp and intense diffraction peaks indicated the high crystallinity of prepared samples. It also showed that the XRD signals of catalysts prepared at 200 °C were weaker than that of 180 °C, suggesting the better crystallinity of samples obtained at 180 °C. The influence of reaction time on the catalysts' phase structures is illustrated in Fig. S1. With the lasting reaction time, the crystalline phase of $BiPO_4$ changed from hexagonal to monoclinic. The average crystalline size of the $BiPO_4$ powders was calculated with the Scherer equation and summarized in Table S1. It showed that the relatively higher hydrothermal temperature or longer reaction time resulted in the formation of larger particles [20]. In this study, the $BiPO_4$ photocatalysts synthesized at 180 °C for 72 h were denoted as BPO-180-72.

The typical temperature- and time-dependent FESEM and TEM images of the $BiPO_4$ were presented in Figs. 2, S2 and S3, which describes the obvious evolution in the morphology and size of the $BiPO_4$ products. The high resolution TEM images (Fig. S3e and S3f) of $BiPO_4$ prepared at 180 °C for 72 h indicated the high crystallinity of the samples, which was consistent with the XRD analysis. $BiPO_4$ products were composed of nanorods with diameters from 60 to 100 nm and lengths from 0.1 to 0.3 μm under experimental conditions of lower temperature and shorter reaction time. With increasing temperatures (≥180 °C) or prolonged reaction times (≥48 h), the nanorods were destroyed and the sheet-like shape with explicit cutting edges were formed. However, as the temperature reached 200 °C, or reaction time approached 96 h, the relatively ordered shape of BPO-180-72 broke down (Figs. 2e and S2h). Fig. 3 depicts the possible formation mechanism of $BiPO_4$ nanocrystals, that the growth of the $BiPO_4$ catalysts followed a three-stage growth model [18]. The chemical composition of BPO-180-72 was confirmed by energy dispersive X-ray analysis (Fig. 2f), which revealed that the atomic ratio of bismuth, phosphorus and oxygen was approximately 1:1:4. The selected area electron diffraction (SAED) patterns of the $BiPO_4$ products prepared at different temperatures demonstrated the well-crystallized single phase of the samples (inset of Fig. S3), and further confirmed the results of the XRD analysis. It was worthy to note that the intrinsic crystal structure of $BiPO_4$ may induce the morphology change [21], thus, with the reaction time prolonged to 48 h, the hexagonal phase nanorods turned into disordered monoclinic sheet-like $BiPO_4$ crystals. As the reaction time increased to 72 h, the disordered samples grew to a relatively perfect sheet-like shape. When the reaction time was extended to 96 h, the ordered sheet-like microstructure started to be disintegrated.

N_2 adsorption–desorption tests were performed to investigate the adsorption capacities and pore structures of the $BiPO_4$ samples prepared at various temperatures, and the experimental results were presented in Table S2. As the results revealed, the $BiPO_4$ catalysts prepared at 180 °C had the highest specific surface area, which can facilitate the photocatalytic degradation process via the adsorption of compounds and transmittance of light. Fig. 4 illustrates the UV–vis diffuse reflectance spectra of the $BiPO_4$ catalysts. $BiPO_4$ samples showed obvious photo-absorption at wavelengths lower than 300 nm, which allowed the $BiPO_4$ catalysts to utilize enough light under UV irradiation during the photocatalytic process. The steep shape and strong absorption in the UV region indicated that the light absorption was not due to the transition from the impurity level but to the intrinsic band-gap transition between the valence band and the conduction band [18]. The band gap energy (Eg) of the products was estimated by the following equation [15]:

$$\mathrm{Eg} = \frac{hc}{\lambda_0} \approx \frac{1240}{\lambda_0}$$

where Eg, h, c, λ_0 are band gap energy (eV), Plank constant, velocity of light and maximum absorption wavelength, respectively. The absorption edges of the $BiPO_4$ samples ranged from 279 to 15 nm, corresponding to the Eg of about 3.94–4.44 eV. Eg of BPO-180-72, for instance, was calculated from the onset of the absorption edge to be 4.00 eV (inset of Fig. 4B). With the increase of hydrothermal temperature (≥180 °C) or reaction time (≥48 h), the corresponding UV–vis diffuse reflectance spectroscopy (DRS) spectrum showed a slight red shift, which was likely ascribed to the changes in crystallite phase and size of the $BiPO_4$ samples [21].

The XPS spectra of $BiPO_4$ catalysts are displayed in Fig. S4, which illustrates that the synthesized $BiPO_4$ samples were composed of elements Bi, P, O and C, and no other element was observed. The atomic ratio of Bi, P and O was again confirmed to be 1:1:4 by XPS analysis. The presence of C was likely attributed to the adventitious elemental carbon on the surface of the sample, or the carbon tape used by the XPS technique [22]. Fig. 5 shows the high-resolution XPS spectra of BPO-180-72 (Bi, P and O). The binding energies of Bi 4f7/2 and Bi 4f5/2 corresponded to the characteristic peaks of Bi^{3+} in $BiPO_4$ (Fig. 5A). The presence of oxygen vacancies in the $BiPO_4$

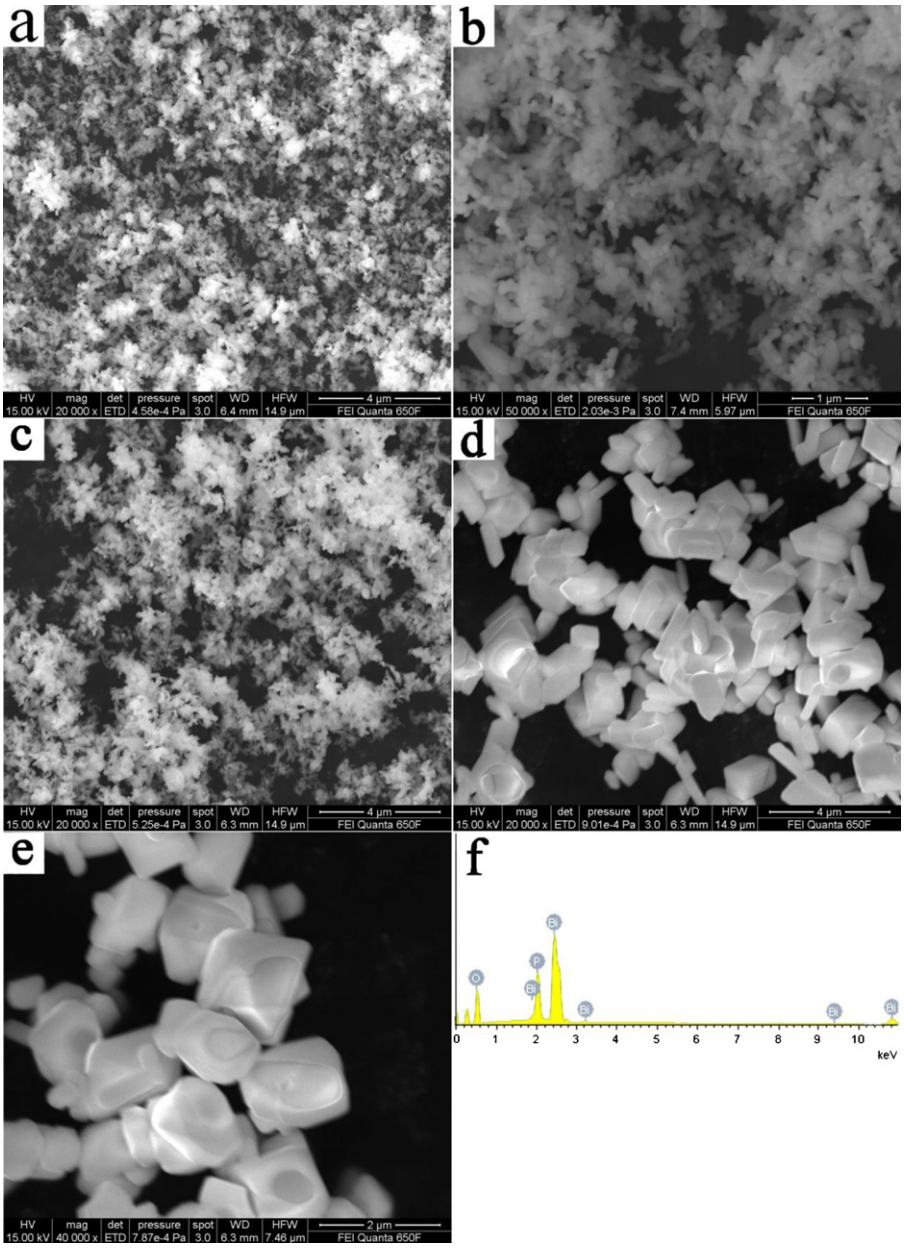

Fig. 2. Typical FESEM images of the $BiPO_4$ nanocrystals fabricated for 72 h at different temperatures: precursor (a); 140 °C (b); 160 °C (c); 180 °C (d) and 200 °C (e) and (f) was the EDX spectrum of $BiPO_4$ synthesized at 180 °C for 72 h.

catalysts prepared at different temperatures was also investigated and the results given in Fig. S5.

The O 1s profile was asymmetric and can be curve-fitted into two Gaussian features, which were assigned to crystal lattice oxygen and chemisorbed oxygen (caused by the surface chemisorbed species, such as $HO^{\bullet}$ and H_2O) with increasing binding energy [9,23]. The percent of adsorbed oxygen over the total oxygen on the surface of the $BiPO_4$ catalysts was calculated to be 41.0%, 45.5%, 39.9% and 42.6% for the products synthesized at 140 °C, 160 °C, 180 °C and 200 °C, respectively, and the results strongly suggested the presence of oxygen deficiencies in the prepared catalysts. It is well known that the existence of oxygen vacancies can promote the photocatalytic process by inhibiting the recombination of the photogenerated electrons and holes [9]. In the present study, the ratios of adsorbed oxygen for the $BiPO_4$ samples prepared at different temperatures were almost the same (with relative standard deviation of 2.4%), thus it was supposed that oxygen vacancies may promote the photodegradation process, but it did not play important roles in the differences of the photocatalytic behaviors of the catalysts prepared at different temperatures.

3.2. Photocatalytic degradation of carbamazepine by $BiPO_4$

The photocatalytic degradation of carbamazepine by $BiPO_4$ catalysts prepared under different hydrothermal temperature and reaction time was investigated, and the removal efficiencies as a function of reaction time are shown in Fig. 6. The photocatalytic processes in the presence of $BiPO_4$ followed the pseudo-first-order reaction:

$$\ln\left(\frac{C_0}{C_t}\right) = kt$$

where C_0 and C_t are the carbamazepine initial equilibrium concentration and reaction concentration at time (t), and k is the reaction

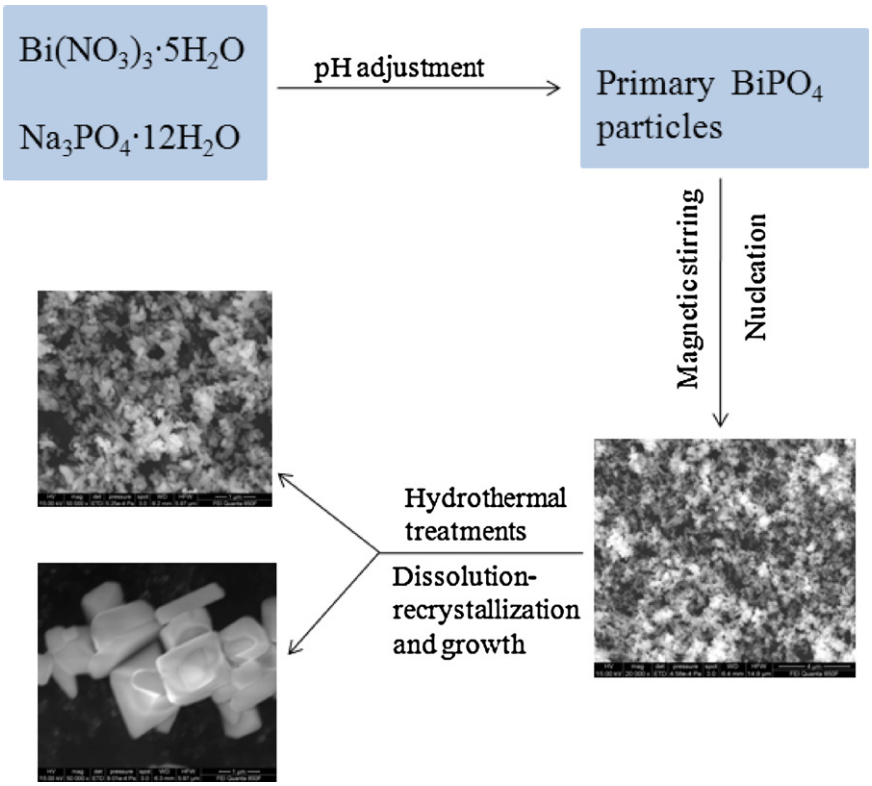

Fig. 3. Schematic illustration for the possible formation mechanism of $BiPO_4$ nanocrystals prepared by hydrothermal treatment.

rate constant (min^{-1}). *k* values were summarized in Table S1, where higher rate constants indicated the stronger photocatalytic activities. Results in Fig. 6A show that degradation efficiencies increased with the increasing hydrothermal temperature from 140 to 180 °C, and reached a plateau at 200 °C, during which nearly all carbamazepine was eliminated. The obvious difference in the photocatalytic performance of carbamazepine by different $BiPO_4$ catalysts suggested that the photocatalytic efficiencies of these $BiPO_4$ were mainly related to their crystal phase, specific surface area, size and morphology. The intrinsic crystal phase of $BiPO_4$ crystals may induce the morphology change from a 1D rod-like microstructure to a 2D sheet-like structure, thus it was speculated that the monoclinic phase was more active than the hexagonal phase for $BiPO_4$ samples.

Fig. 6B displays the photocatalytic activities of $BiPO_4$ prepared with different hydrothermal reaction times. The product synthesized with reaction time of 72 h showed the best removal efficiency of carbamazepine, which was related to the crystal phase and morphology of the catalysts. A previous study showed that the disordered morphology was beneficial for the e^-–h^+ recombination, and resulted in a decrease in photocatalytic activity [15]. Compared with $BiPO_4$ samples prepared for 48 or 96 h, the 72 h-synthesized particle was more ordered in shape, and this feature facilitated the photocatalytic reaction, leading to higher photocatalytic activity. In this study, the optimal preparation condition was determined as a hydrothermal temperature of 180 °C for 72 h, which was referred to as BPO-180-72 above. Its superior activity may be attributed to the combination effect of its monoclinic phase and relatively ordered sheet-like shape.

The photocatalytic degradation of carbamazepine in simulated wastewater under UV light irradiation by BPO-180-72 was also evaluated (Fig. S6), with ultrapure water as the reference media. As shown in Fig. S6 (blank test), less than 20% of carbamazepine was eliminated in the absence of $BiPO_4$ catalysts. In simulated wastewater, 72.4% of carbamazepine was removed after 60 min irradiation, while nearly 100% of carbamazepine was removed in the ultrapure water. The relatively lower removal efficiency of carbamazepine in the simulated wastewater was probably due to the coexistent inorganic and organic species in the simulated wastewater, which may compete with the reactive radicals such as $HO^{\bullet}$ and h^+ with the target compounds, thus resulting in the reduction of removal capabilities [19]. The total organic carbon (TOC) changes as a function of reaction time in simulated wastewater and ultrapure water are given in Fig. S7, which confirmed that mineralization occurred during the process. The result suggested the potential application of $BiPO_4$ for the treatment of organic substances from real wastewater.

3.3. Reaction intermediates and pathway of carbamazepine by BPO-180-72

Time course profiles of HPLC-SIR-MS spectra for carbamazepine by BPO-180-72 under UV irradiation are given in Fig. S8. With the prolonged irradiation time, the peak area of carbamazepine gradually decreased while some new characteristic peaks simultaneously appeared, indicating the effective removal of carbamazepine and the formation of transformation products.

Ten main product ions at *m*/*z* 253.1, 149.0, 259.1, 275.0, 253.1, 253.1, 208.2, 180.1, 301.1 and 349.2 were observed (Fig. S9, Table S3). The products/intermediates were identified by the specific molecular ions, mass fragment peaks as well as the HPLC–MS library data, and the corresponding chemical information was listed in Table S3. The intermediates at *m*/*z* 253.1 (A), 253.1 (F) and 180.1 (H) were previously identified by Ghauch et al., where they detected the intermediates of carbamazepine by improved Fenton oxidation [2]. Using Mn (VII) and Fe (VI) to oxidize carbamazepine, the intermediates at *m*/*z* 259.1 (C) and 301.1 (I) were also observed [8]. Although these intermediates have been reported, as

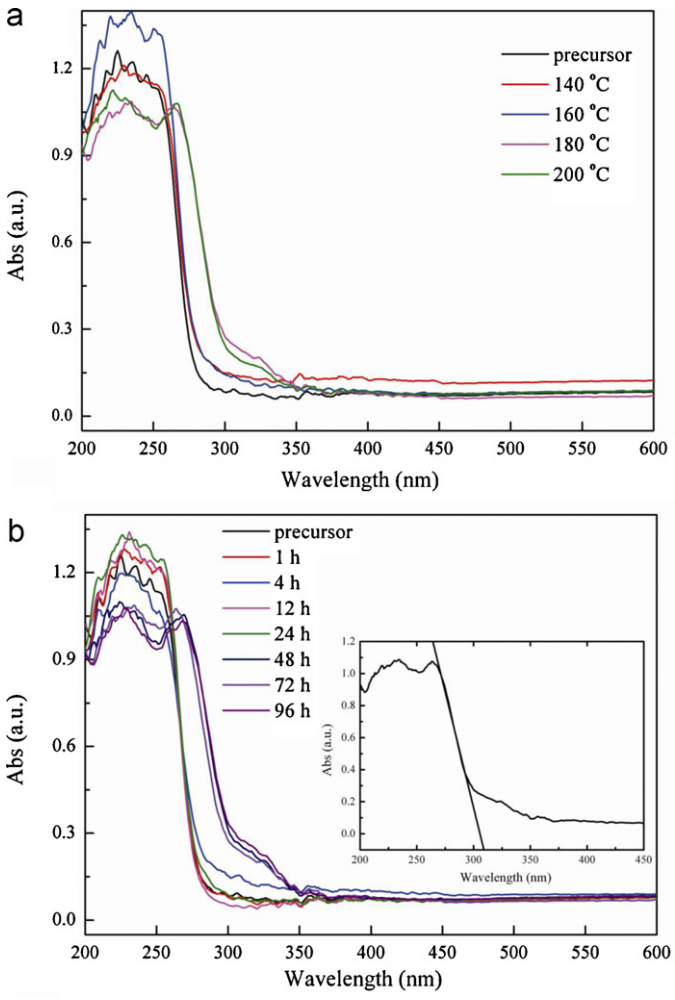

Fig. 4. UV-DRS patterns of $BiPO_4$ samples prepared for 72 h at different temperatures (A) and times (B).

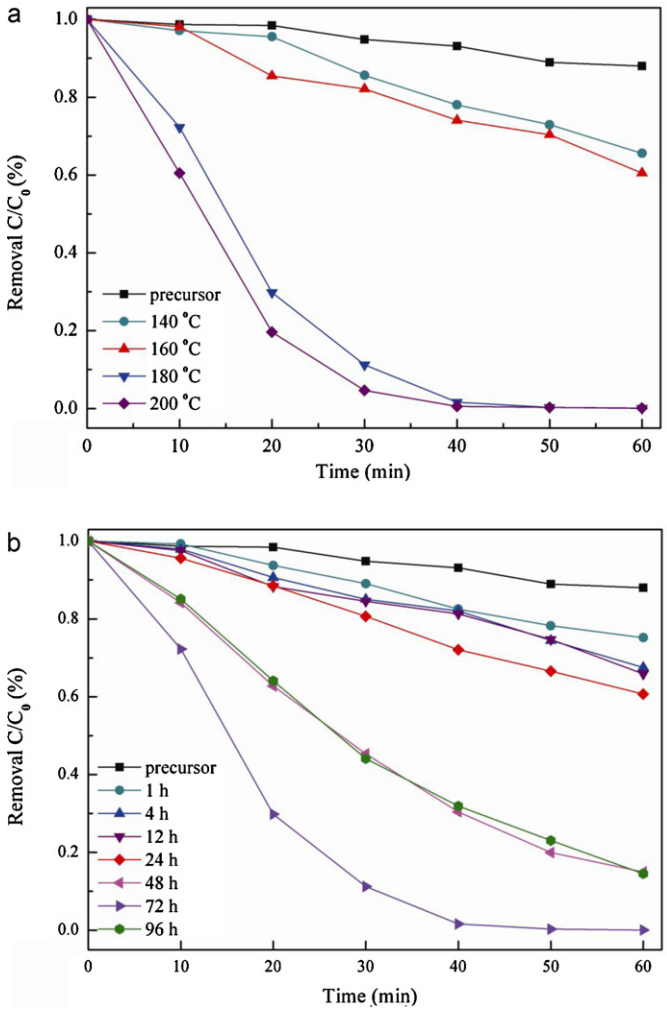

Fig. 6. Photocatalytic degradation of carbamazepine by $BiPO_4$ catalysts prepared at specific temperatures (A) and reaction time (B) under UV light irradiation. The initial carbamazepine concentration was 5.0 mg/L, and catalyst dosage was 1.0 g/L.

far as we know, a study concerning the photodegradation of carbamazepine by $BiPO_4$ nanoparticles has not been reported yet. Three new intermediates that differed from the previously reported compounds were determined in the present study (intermediates at m/z 149.0 (B), 275.1 (D) and 349.2 (J)). The complex hydroxylated intermediates (D and J) elucidated the important role of $HO^{\bullet}$ radicals as reactive species during the photodegradation process [24].

Based on the general rules of photocatalytic oxidation of organic compounds and the intermediates identified by LC–MS, a tentative degradation pathway of carbamazepine by BPO-180-72 was proposed (Fig. 7). The major reactive species involved in the carbamazepine degradation in aqueous $BiPO_4$ suspensions were photogenerated holes and hydroxyl radicals. In aqueous solution, the $HO^{\bullet}$ radicals were mainly formed through the hole capturing HO^- of water or the reduction of O_2 with the electrons [25]. For $BiPO_4$, the standard redox potential of Bi^{III}/Bi^{V} (1.59 eV at pH 0) was lower than that of $HO^{\bullet}/HO^-$ (1.99 eV), thus the $HO^{\bullet}$ on the surface of the $BiPO_4$ catalysts were mainly generated from the reduction of O_2 [16]. Based on our experimental data (fluorescence spectral results, Fig. S10), hydroxyl radicals were formed in the presence of

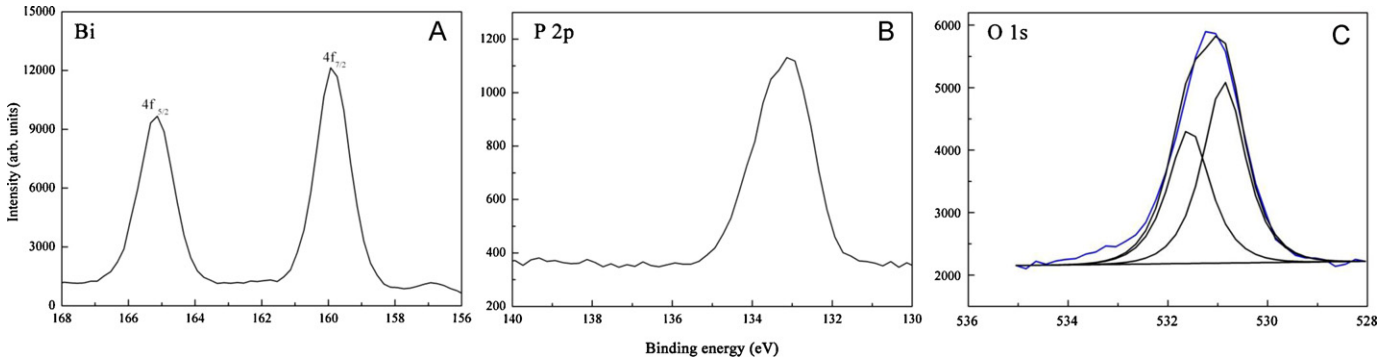

Fig. 5. XPS spectrum of $BiPO_4$ prepared at 180 °C for 72 h.

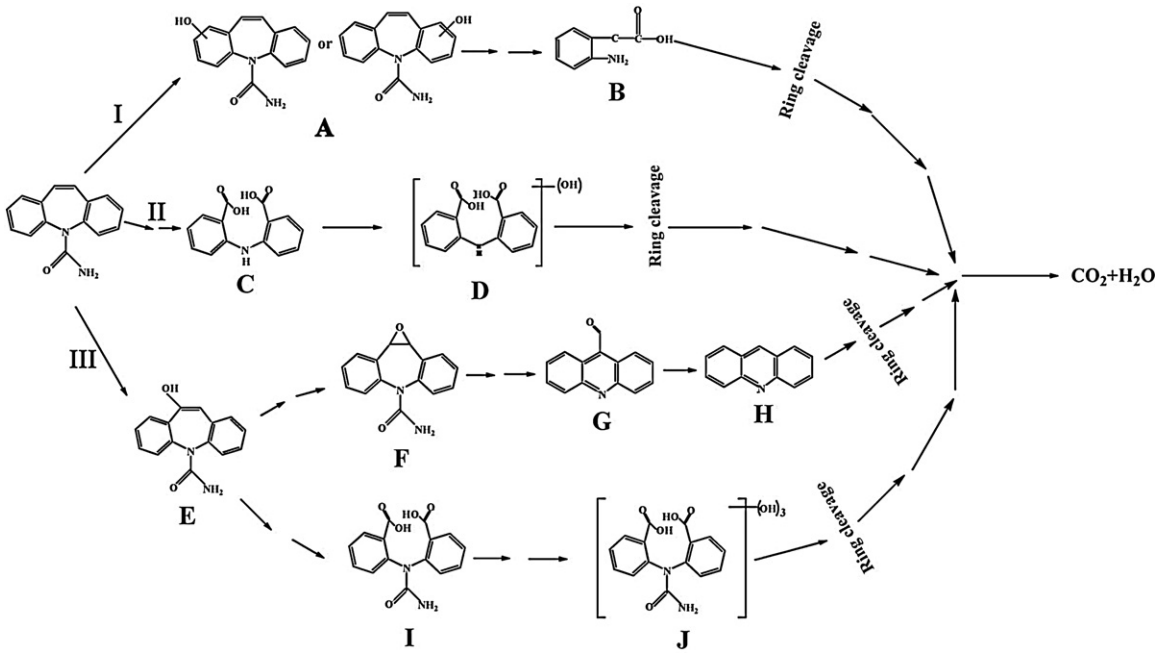

Fig. 7. Proposed degradation pathway of carbamazepine by BPO-180-72 under UV light irradiation. The initial carbamazepine concentration was 5.0 mg/L, and catalyst dosage was 1.0 g/L.

$BiPO_4$ catalysts under UV light irradiation. First of all, the generated HO• directly reacted with carbamazepine and formed compounds A and E (pathways I and III). During the photocatalytic process, hydroxylation of aromatic rings by HO• radicals was reported to be an important reaction in the sequential ring cleavage reactions [15,16,20]. Therefore, the HO• attacked the olefinic double bond on the central heterocyclic ring, which was further oxidized through a ring-rupturing reaction by photogenerated holes to generate product C (pathway II). Further oxidation of intermediate A by the holes produced the relatively low-molecular-weight compound B. Meanwhile, compound E underwent two different ways in the following reactions. With the attack of HO· at the olefinic double bond on the central heterocyclic ring and an elimination process, product F was formed, which then underwent a hydrogen rearrangement reaction, leading to the generation of compound G. Subsequently, the intermediate G was presumably further oxidized through incision into compound H. In tandem with that process, product E was transformed to compound I, which was similar to pathway II. In the transformation process, hydroxylation played important roles. With the existence of HO• radicals, the intermediates C and I could be oxidized to complex hydroxylated intermediates D and J, however, no exact position for hydroxyl groups could be proposed from the fragmentation pattern. Finally, the complex hydroxylated intermediates (D and J) and low molecular compounds (B and H) were oxidized through ring-rupturing reactions to aliphatic compounds, which upon further oxidation were mineralized to benign CO_2 and HO_2 [26]. Generally, carbamazepine degradation by monoclinic phase $BiPO_4$ under UV light irradiation was mainly driven by photogenerated holes and HO• radicals oxidation, which simultaneously led to the complete mineralization of the pollutant. The newly found complex hydroxyl compounds D and J confirmed the participation of nonselective HO• radicals during the degradation process.

4. Conclusion

$BiPO_4$ photocatalysts were controllably prepared by a one-step hydrothermal method with the adjustment of hydrothermal temperature and reaction time, which were demonstrated to affect the crystallite phase, morphology and optical abilities of the $BiPO_4$ catalysts. The catalyst prepared at 180 °C for 72 h exhibited high photocatalytic performance for the photodegradation of carbamazepine both in the ultrapure water and in the simulated wastewater, and the high photocatalytic activity may be attributed to the combined effect of its monoclinic phase and relatively ordered sheet-like shape. With the help of HPLC/MS/MS analysis, ten main reaction intermediates/products were identified, and the degradation process was dominated by the photogenerated holes and HO• radicals.

Acknowledgement

This work was financially supported by National Natural Science Foundation of China (20977051).

Appendix A. Supplementary data

Time-dependent XRD, FESEM images, TEM, XPS spectra, simulated wastewater degradation, chromatographs by LC/MS, and detailed *m*/*z* spectra are given in Figs. S1–S10. The physiochemical properties of $BiPO_4$ and intermediates information are described in Tables S1 and S3.

Supplementary data associated with this article can be found, in the online version, at http://dx.doi.org/10.1016/j.apcatb.2012.11.013.

References

[1] G. Arye, I. Dror, Chemosphere 82 (2011) 244–252.
[2] A. Ghauch, H. Baydoun, P. Dermesropian, Chemical Engineering Journal 172 (2011) 18–27.
[3] S.B. Abdelmelek, J. Greaves, K.P. Ishida, W.J. Cooper, W.H. Song, Environmental Science and Technology 45 (2011) 3665–3671.
[4] W.H. Zhang, Y.J. Ding, S.A. Boyd, B.J. Teppen, H. Li, Chemosphere 81 (2010) 954–960.
[5] T. Kosjek, H.R. Andersen, B. Kompare, A. Ledin, E. Heath, Environmental Science and Technology 43 (2009) 6256–6261.
[6] C.F. Williams, C.F. Williams, F.J. Adamsen, Journal of Environment Quality 35 (2006) 1779–1783.

[7] M.M. Huber, S. Canonica, G. Park, U.V. Gunten, Environmental Science and Technology 37 (2003) 1016–1024.
[8] L. Hu, H.M. Martin, O. Arce-bulted, M.N. Sugihara, K.A. Keating, T.J. Strathmann, Environmental Science and Technology 43 (2009) 509–515.
[9] L.W. Zhang, T.G. Xu, X. Zhao, Y.F. Zhu, Applied Catalysis B 98 (2010) 138–146.
[10] Z.J. Zhang, W.Z. Wang, E.P. Gao, M. Shang, J.H. Xu, Journal of Hazardous Materials 196 (2011) 255–262.
[11] K.S. Hu, X. Xiao, X.F. Cao, R. Hao, X.X. Zuo, X.J. Zhang, J.M. Nan, Journal of Hazardous Materials 192 (2011) 514–520.
[12] K.D. Witte, A.M. Busuioc, V. Meynen, M. Mertens, N. Bilba, G.V. Tendeloo, P. Cool, E.F. Vansant, Microporous and Mesoporous Materials 110 (2008) 100–110.
[13] D.J. Wang, G.L. Xue, Y.Z. Zhen, F. Fu, D.S. Li, Journal of Materials Chemistry 22 (2012) 4751.
[14] C.S. Pan, Y.F. Zhu, Environmental Science and Technology 44 (2010) 5570–5574.
[15] C.Y. Wang, L.Y. Zhu, C. Song, G.Q. Shan, P. Chen, Applied Catalysis B 105 (2011) 229–236.
[16] J. Xu, W. Meng, Y. Zhang, L. Li, C.S. Guo, Applied Catalysis B 107 (2011) 355–362.
[17] G.F. Li, Y. Ding, Y.F. Zhang, Z. Lu, H.Z. Sun, R. Chen, Journal of Colloid and Interface Science 363 (2011) 497–503.
[18] C.S. Pan, Y.F. Zhu, Journal of Materials Chemistry 21 (2011) 4235.
[19] C. Postigo, C. Sirtori, I. Oller, S. Malato, M.I. Maldonado, M.L. Alda, D. Barceló, Applied Catalysis B 104 (2011) 37–48.
[20] Y.C. Feng, L. Li, M. Ge, C.S. Guo, J.F. Wang, L. Liu, Applied Materials and Interfaces 2 (2010) 3134–3140.
[21] M. Shang, W. Wang, L. Zhang, Journal of Hazardous Materials 167 (2009) 803–809.
[22] Z. Ai, W. Ho, S. Lee, L. Zhang, Environmental Science and Technology 43 (2009) 4143–4150.
[23] L.Q. Jing, X.J. Sun, B.F. Xin, B.Q. Wang, W.M. Cai, H.G. Fu, Journal of Solid State Chemistry 77 (2004) 375–382.
[24] Y.F. Rao, W. Chu, Environmental Science and Technology 43 (2009) 6183–6189.
[25] Y.S. Cao, L. Yi, L. Huang, Y. Hou, Y.T. Lu, Environmental Science and Technology 40 (2006) 3373–3377.
[26] Q. Wang, B. Geng, S. Wang, Environmental Science and Technology 43 (2009) 8968–8973.